Macromolecular Bioscience
www.mbs-journal.de

Bioprinting of Human Liver-Derived Epithelial Organoids for Toxicity Studies

*Manon C. Bouwmeester, Paulina N. Bernal, Loes A. Oosterhoff, Monique E. van Wolferen, Vivian Lehmann, Monique Vermaas, Maj-Britt Buchholz, Quentin C. Peiffer, Jos Malda, Luc J. W. van der Laan, Nynke I. Kramer, Kerstin Schneeberger, Riccardo Levato, and Bart Spee**

There is a need for long-lived hepatic in vitro models to better predict drug induced liver injury (DILI). Human liver-derived epithelial organoids are a promising cell source for advanced in vitro models. Here, organoid technology is combined with biofabrication techniques, which holds great potential for the design of in vitro models with complex and customizable architectures. Here, porous constructs with human hepatocyte-like cells derived from organoids are generated using extrusion-based printing technology. Cell viability of bioprinted organoids remains stable for up to ten days (88–107% cell viability compared to the day of printing). The expression of hepatic markers, transporters, and phase I enzymes increased compared to undifferentiated controls, and is comparable to non-printed controls. Exposure to acetaminophen, a well-known hepatotoxic compound, decreases cell viability of bioprinted liver organoids to 21–51% ($p < 0.05$) compared to the start of exposure, and elevated levels of damage marker miR-122 are observed in the culture medium, indicating the potential use of the bioprinted constructs for toxicity testing. In conclusion, human liver-derived epithelial organoids can be combined with a biofabrication approach, thereby paving the way to create perfusable, complex constructs which can be used as toxicology- and disease-models.

1. Introduction

Drug-induced liver injury (DILI) is the most frequent reason for drug failure in clinical trials and post-marketing drug withdrawal.[1] Thirty percent of drug candidates are discontinued due to hepatic dysfunction even post-marketing.[2] Additionally, drug-induced liver injury accounts for more than fifty percent of the cases of acute liver failure in the United States.[3] Preclinical drug testing using rodent models allow for drug evaluation in the presence of a complete immune system and cross-talk with other organs.[4] However, significant inter-species differences in metabolic processes, disease mechanisms, and modes of toxicity, hamper the extrapolation of obtained preclinical data to the human situation.[5,6]

Compared to animal models, human hepatic in vitro models could give more insight in specific metabolic processes and mechanisms of toxicity, and allow for an

M. C. Bouwmeester, L. A. Oosterhoff, M. E. van Wolferen, V. Lehmann, M. Vermaas, M.-B. Buchholz, J. Malda, K. Schneeberger, R. Levato, B. Spee
Department of Clinical Sciences
Faculty of Veterinary Medicine
Regenerative Medicine Center Utrecht
Utrecht University
Uppsalalaan 8, Utrecht 3584 CT, The Netherlands
E-mail: b.spee@uu.nl

P. N. Bernal, Q. C. Peiffer, J. Malda, R. Levato
Department of Orthopaedics
Regenerative Medicine Center Utrecht
University Medical Center Utrecht
Uppsalalaan 8, Utrecht 3584 CT, The Netherlands

V. Lehmann
Division of Pediatric Gastroenterology
Wilhelmina Children's Hospital
Regenerative Medicine Center Utrecht
Uppsalalaan 8, Utrecht 3584 CT, The Netherlands

L. J. W. van der Laan
Department of Surgery
Erasmus Medical Center
Postbus 2040, Rotterdam 3000 CA, The Netherlands

N. I. Kramer
Institute for Risk Assessment Sciences
Utrecht University
Yalelaan 2, Utrecht 3584 CM, The Netherlands

N. I. Kramer
Division of Toxicology
Wageningen University
P.O. box 8000, Wageningen 6700 EA, The Netherlands

The ORCID identification number(s) for the author(s) of this article can be found under https://doi.org/10.1002/mabi.202100327

DOI: 10.1002/mabi.202100327

ethically less controversial model.[7] Primary human hepatocytes (PHHs) are considered the golden standard due to the representative expression levels of metabolizing enzymes and expression of liver-specific markers. However, PHHs rapidly dedifferentiate leading to decreased hepatic function in vitro and the availability of these cells is limited.[8] Nevertheless, PHHs are still widely used and recently introduced culture strategies are able to delay the dedifferentiation process in an attempt to set up a model that can be used for long-term toxicity testing.[9–11] To overcome previously mentioned limitations of PHHs, hepatic cell lines, such as HepG2 and HepaRG, are extensively used.[12] Although advantages of hepatic tumor-derived lines include their availability and nearly unlimited growth, they generally have reduced expressions of key hepatic enzymes compared to PHHs.[13] Similar to PHHs, new culture strategies exist that are able to improve the hepatic function,[14] however these cell lines are single-donor-derived and therefore do not exhibit interindividual differences. Especially in the case of the liver, a model needs to recapitulate the interindividual variation in metabolism, which is a major contributor to heterogeneity in drug clearance.[15]

Organoids have a great potential to serve as liver models as they recapitulate aspects of the native tissue architecture and function in vitro.[16] Organoids are cultured as 3D structures that are derived from primary cells (stem cells, progenitor, and/or differentiated cells) that self-organize through cell–cell and cell–matrix interactions.[17] Epithelial organoids are single germ layer derived and under specific culture conditions, expand and polarize to reproduce aspects of the native epithelium.[18] In the case of the liver, progenitor cells derived from the biliary tree can be cultured as organoids and differentiated into the cholangiocytic- and hepatocytic-lineage indicating a true bipotential nature. In culture conditions where the Wnt/b-catenin pathway is induced, these progenitor cells from the intrahepatic biliary tree form organoids (intrahepatic cholangiocyte organoids, ICOs) and upregulate stem cell marker leucine-rich repeat-containing G-protein coupled receptor 5 (LGR5).[19] ICOs are highly proliferative, expanding as cystic structures for several months while remaining genetically stable and can be produced in large scale.[20,21] Under differentiating conditions ICOs upregulate hepatocyte markers and acquire mature hepatocyte functions, such as albumin and bile acid secretion, glycogen storage, phase I and II drug metabolism, and ammonia detoxification.[20] Unlike cellular aggregates or spheroids, the organoids are cystic-like structures which, in the case of hepatic differentiation, are polarized with the apical side at the inside, facing the organoid lumen.[21] As ICOs are donor-derived, they can reflect interindividual variability in metabolic activity in vitro. Current hepatic maturity is limited compared to primary hepatocytes as indicated by lower hepatic function (e.g., albumin expression and cytochrome activity).[20] In order to improve hepatic maturation, the complexity of the in vitro constructs can be increased, thereby more closely mimicking the native liver environment.[22] Biofabrication techniques, and more specifically bioprinting, can provide such complexity through the precise placement of biomaterial inks or bioinks to promote cellular interactions, and through the production of constructs that allow for vascularization and enhanced exchange of nutrients.[23,24]

The potential to converge bioprinting and self-assembled biological building units like organoids, has recently sparked attention in the biofabrication field, due to the possibility to create models at the tissue-like level scale.[25,26] Hence, novel models that benefit from both the 3D spatial control, as provided by bioprinting, and of the biological resemblance by using organoids as building blocks and bioink components, holds great potential to introduce a humanized testing platform for personalized medicine and drug screening. Here, we take the initial step toward increasing the culture complexity of human ICOs by showing that bioprinted organoids can be processed into functional liver constructs.

2. Results

Hepatic constructs were created with extrusion-based bioprinting using organoid-derived hepatocyte-like cells and gelatin-based hydrogel (GelMA) as a bioink. After expanding the intrahepatic cholangiocyte organoids (ICOs) in Matrigel, in order to achieve the cell amount required for the bioprinting of the liver constructs, ICOs were resuspended in GelMA at a 2–5 million cells per mL density. Cell-laden GelMA was co-printed with the sacrificial hydrogel Pluronic-127 allowing to create porous constructs (**Figure 1**a). Printed constructs consisted of printed strands of 600 to 1,000 μm with pores of 200 to 400 μm in size (Figure 1b). Diffusion through the GelMA hydrogel occurred at >1,000 μm within minutes, as was determined by using a coloring dye (Figure S1, Supporting Information). This observation indicates that the hydrogel allows an exchange of soluble compounds with molecular weight comparable or superior to the drugs used in this work, thus permitting exposure to the hydrogel-embedded organoids. Moreover, the shear thinning property of GelMA was unaffected by the presence of organoids in the hydrogel (Figure S1, Supporting Information), as the trend in viscosity with increasing angular frequency was comparable to GelMA without organoids.

2.1. Cell Viability in Bioprinted Constructs

Hepatic differentiation of ICOs was started directly after bioprinting using differentiation media. After 10 days of culture, morphology of the organoids was assessed using an HE staining. We observed that the organoids remained within the printed GelMA struts or aligned along the edge (Figure 1c) with an average diameter size of 48.2 ± 29.0 μm (Figure S2, Supporting Information). Organoids were distributed evenly throughout the construct with an overall coverage area of 6.4 ± 0.4% (Figure S2, Supporting Information) of bioprinted struts. In order to assess if the printed constructs can be applied for long-term toxicity studies, we assessed the cell viability of organoids over time using an Alamar blue assay as well as a live-dead assay. The differentiated (non-proliferative) organoids remained viable over a period of 10 days (≈88–107% cell viability compared to printing day; Figure 1d) as determined using an Alamar blue assay, which is comparable to organoids plated in GelMA (non-printed). Fluorescence imaging of live/dead cells showed that the amount of viable cells is stable over time and individual dead cells, which are present on the first day after printing, decreased over time (Figure 1e), which is comparable to the plated control (data not shown).

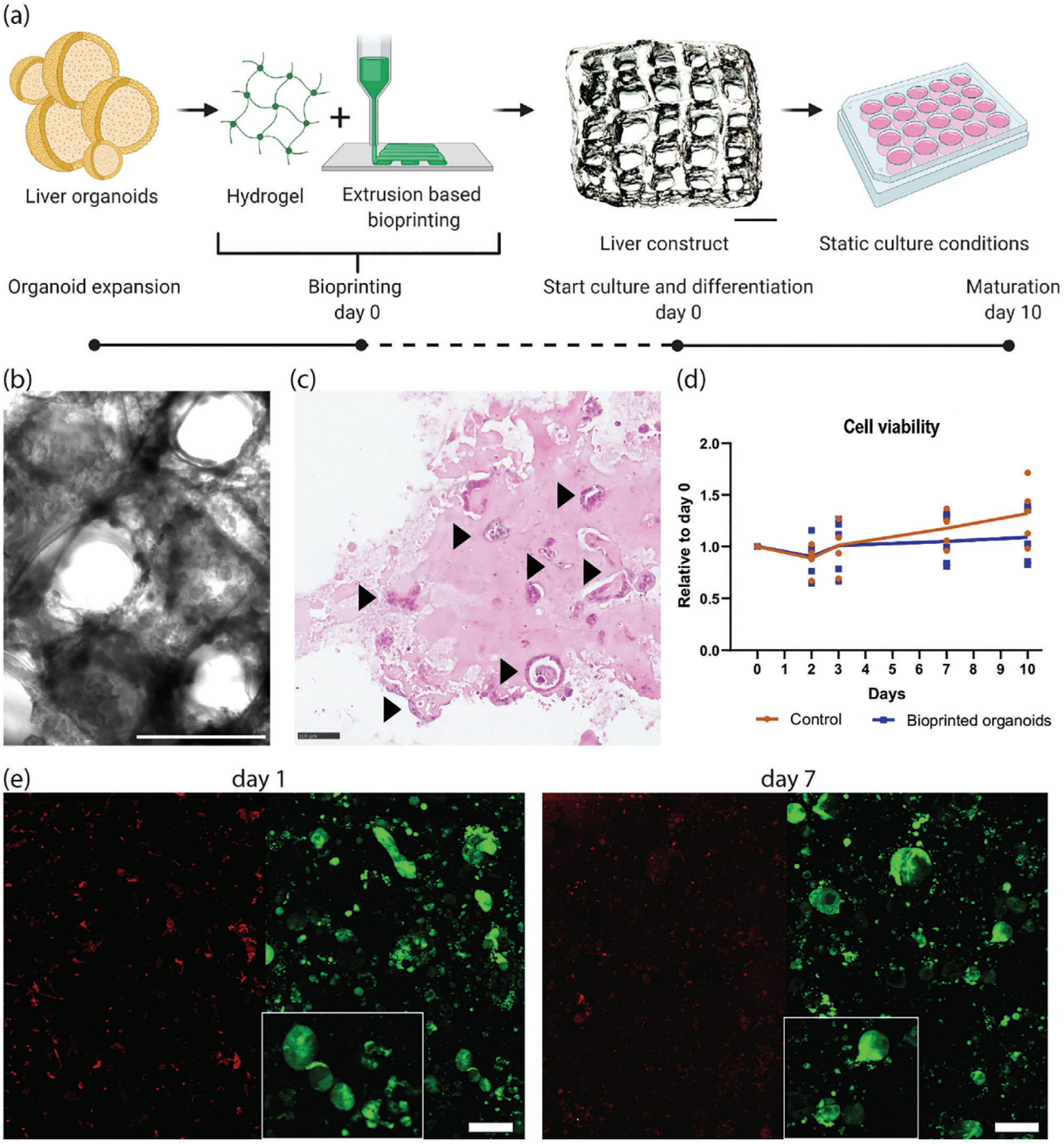

Figure 1. Bioprinting liver constructs. a) Schematic overview of the experimental procedure for bioprinting liver constructs. Once expanded, liver organoids (ICOs) are encapsulated in hydrogel (GelMA). A porous construct is fabricated using extrusion-based bioprinting of the bioink. The construct is cultured in organoid differentiation media, thus guiding organoids toward a hepatocyte-like phenotype. Scale bar = 1,000 µm. Created with BioRender.com b) Brightfield image of the bioprinted liver construct. Scale bar = 1,000 µm. c) HE staining of the bioprinted liver construct. Scale bar = 100 µm. Arrowheads indicate cystic organoid structures within printed struts. Scale bar = 100 µm, inserts are twofold higher magnification. d) Cell viability of liver organoids in GelMA (five donors) after plating (control; orange) and after printing (blue). Each dot represents the mean of a technical triplicate of a single donor. e) Representative image of the live/dead staining of liver organoids after printing at days 1 and 7 post-printing. Viable cells are stained in green, dead cells in red; image covers an entire printed strut.

2.2. Post-Printing Hepatic Functionality

Hepatic differentiation of the organoids in GelMA droplets and extrusion-based bioprinted constructs was compared to organoids in plated Matrigel cultures (day 10 of differentiation) by gene expression profiling and protein expression (immunofluorescence). As expected, gene expression profiling indicated a decrease of the stemness marker leucine-rich repeat-containing G-protein coupled receptor 5 (*LGR5*) compared to expansion conditions ($p < 0.01$ for plated and printed organoids), and an increase of hepatic markers ATP-binding cassette super-family G member 2 (*G6PC*), bile salt export pump (*BSEP*), glucose-6-phosphatase catalytic subunit (*ABCG2*), and *cytochrome P450 3A4* (*CYP3A4*) in differentiation conditions compared to expansion conditions (**Figure 2**a). Expression levels of albumin, *G6PC*, *ABCG2*, and *CYP3A4* and cytochrome P450 2E1 (*CYP2E1*) show that organoids have donor-to-donor variation, with one of the donors showing low expression, whereas the other donors show increased expression levels in differentiation condition (Figure 2a). Overall, GelMA differentiating conditions (both printed constructs and plated controls) showed similar gene expression levels for the hepatic markers compared to Matrigel. Immunofluorescence analysis (Figure 2b) showed that the cytoskeleton marker CK18 (cytokeratin 18) is present in bioprinted liver constructs (Figure S3, Supporting Information). Expression of membrane marker E-cadherin and tight junction marker zonula occludens-1 (ZO-1; Figure S3, Supporting Information) confirm that the bioprinted organoids retain an epithelial phenotype. Additionally, expression of hepatic markers HNF4α (hepatic nuclear factor 4 alpha), albumin, and argininosuccinate synthase (ASS) show differentiation toward hepatocytes. Expression of multi drug resistance protein 1 (MDR1), an apical transporter, shows polarization of liver organoids, allowing for transepithelial transport. Another characteristic of hepatocytes is glycogen storage. Glycogen can be hydrolyzed during a fasting state to generate glucose. Periodic acid-Schiff staining for glycogen shows that bioprinted organoids show glyocogen accumulation indicating hepatic function (Figure 2c).

2.3. Toxicity in Bioprinted Constructs

As a proof-of-concept that the liver constructs can be applied to predict drug toxicity, we exposed bioprinted human organoids (five donors) to the well-known hepatotoxic compound acetaminophen (APAP) on post-printing (differentiation) day 7 (72 h to 30 mM). APAP can cause liver toxicity after biotransformation into its toxic metabolite N-acetyl-p-benzoquinone imine (NAPQI) by cytochrome P450 enzymes. Exposed organoids had a decreased cell viability to 21–45% ($p < 0.01$) after 72h of exposure compared to the start of exposure (**Figure 3**a), which is comparable to APAP toxicity observed in non-printed organoids (Figure S4, Supporting Information). Fluorescence imaging of cell viability shows that after 72 h of APAP exposure, the spherical shape of the organoids is disrupted indicating cellular stress (Figure 3b). Additionally, levels of damage marker miRNA-122 were also measured for four donors in the media. Levels of miRNA-122 was elevated compared to non-exposed organoids indicating leakage of miRNA–122 into the media (Figure 3c). Taken together, this data suggests that bioprinted organoids contain functional cytochrome P450 enzymes which were able to biotransform APAP into its toxic metabolite NAPQI.

3. Discussion

The present study shows the potential application of hepatocyte-like cells derived from human intrahepatic cholangiocyte organoids (ICOs) for the bioprinting of drug responsive liver models. This enables the production of liver tissue constructs that are able to metabolize compounds relevant for pharmaceutical research. To obtain such models, an extrusion-based bioprinting strategy using an organoid-laden, gelatin-based bioink was established. Bioprinted hepatocyte-like cells from ICOs with a sustained metabolic activity provide possibilities for developing more advanced post-printing culture platforms, such as bioreactors and the incorporation of microfluidic devices, which will increase functional maturation, as well as standardized testing procedures.[16,27,28] Herein, it is demonstrated that hepatic functionality of differentiated ICOs in GelMA (plated and bioprinted) is comparable to regular Matrigel cultures. As a proof of principle to show the potential of bioprinted hepatocyte-like cells from ICOs to predict in vitro toxicity, bioprinted constructs were exposed to acetaminophen (APAP), a well-known hepatotoxic drug.[29] Donor-derived liver organoids are hollow cystic structures that express hepatic functionality once differentiated toward the hepatic lineage.[20] After differentiation, the hepatocyte-like cells are polarized as indicated by specific membrane transporters at either the apical or basolateral membrane. The observed polarization (MDR1), an apical membrane transporter, does mimic the native tissue in great detail and is important in the excretion of metabolites and transepithelial transport which can be measured in the media surrounding the bioprinted construct. In non-polarized 2D cultures, such transport studies are not possible.[30] The donor-derived origin of the liver organoids was visible in our expression profile as not all donors showed similar expression levels, such as CYP3A4 and CYP2E1. Interindividual differences in metabolic gene expression profile may contribute to the sensitivity to hepatotoxic drugs,[31] a feature that single-donor derived hepatic cell lines do not provide.[12]

Additionally to toxicity screening, hepatocyte-like cells from ICOs also hold great promise for therapeutic applications due to their patient-derived origin. Next to iPSCs, it is one of the few models that allow for precision medicine approaches.[32] Tissue-derived epithelial organoids have been shown to exhibit patient-specific phenotypes in vitro,[33] thereby enabling personalized testing of therapeutic applications. Disease modeling using patient derived liver organoids has been described for diseases such as Alagille syndrome and alpha-1 antitrypsin deficiency.[20] Moreover, patient-derived organoids have been show to allow for genetic repair by gene editing techniques[34] and are envisioned as a clinical therapy.[35] Next to the liver-derived organoids focused on in this paper, the described bioprinting strategy can also be used in combination with tissue-derived organoids from other organs, including gall bladder, kidney, intestine, and pancreas[36–38] paving the way for more in vitro (disease) modeling opportunities.

Although hepatocyte-like cells from ICOs are a valuable tool for studying metabolism, even after differentiation some hepatic

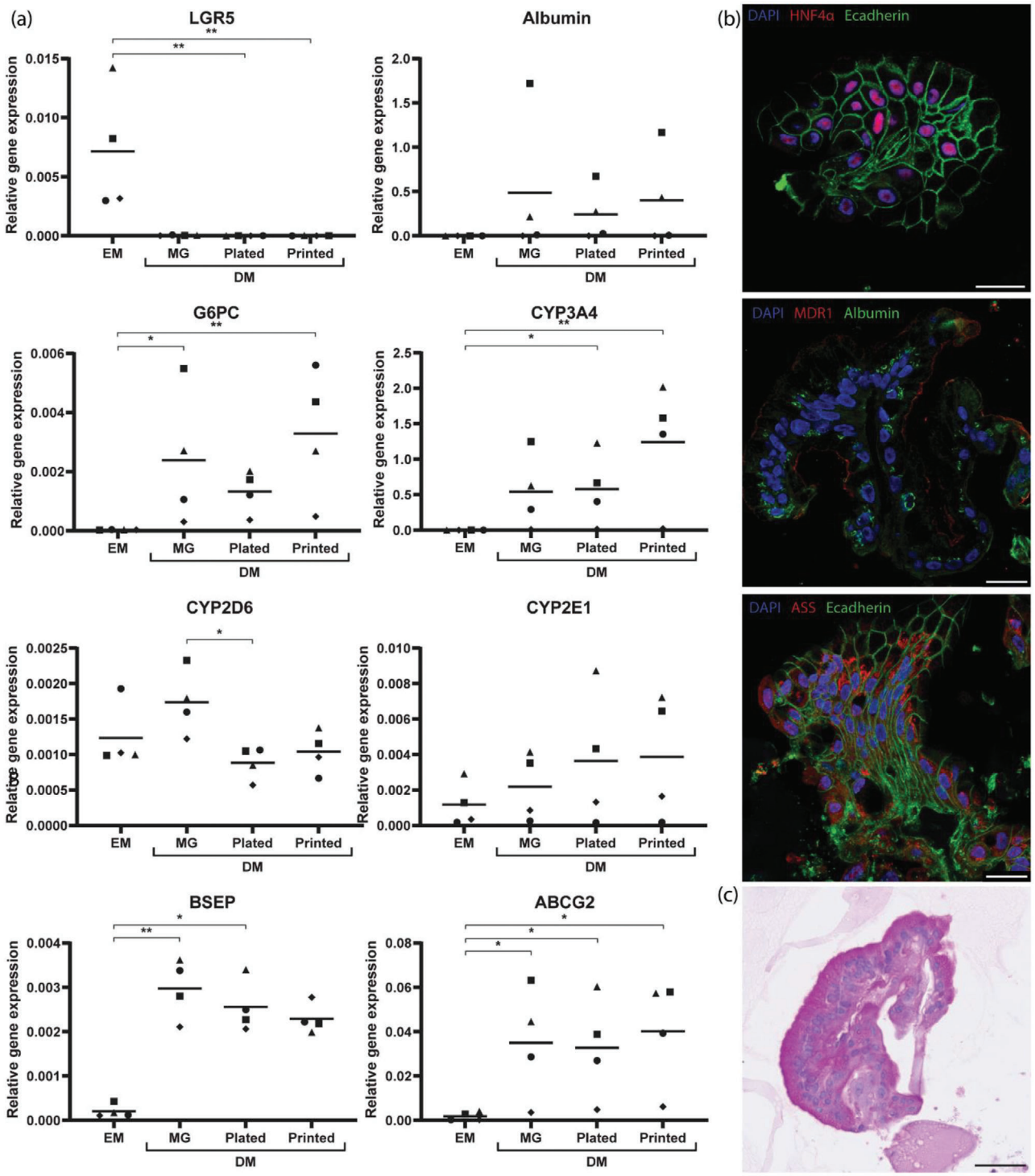

Figure 2. Functionality assessment in liver constructs. a) Gene expression of liver organoids (ICOs) in Matrigel (MG; expansion (EM) and differentiation (DM) conditions), plated and printed in GelMA in differentiation conditions (DM). Each dot represents the mean of a technical triplicate of a single donor. Relative gene expression was calculated using the reference genes *GAPDH* and *RPS5* (ΔCt). *LGR5*, Leucine-rich repeat-containing G-protein coupled receptor 5; *G6PC*, ATP-binding cassette super-family G member 2; *CYP2D6*, Cytochrome P450 2D6; *CYP3A4*, Cytochrome P450 3A4; *CYP2E1*, Cytochrome P450 2E1; *ABCG2*, Glucose-6-Phosphatase Catalytic Subunit; *BSEP*, Bile salt export pump b) Immunofluorescence staining in liver constructs. Scale bar = 25 µm. HNF4α, Hepatocyte nuclear factor 4 alpha; MDR1, multidrug resistance protein 1; ASS, argininosuccinate synthase c) Glycogen accumulation in liver construct. Scale bar = 50 µm.

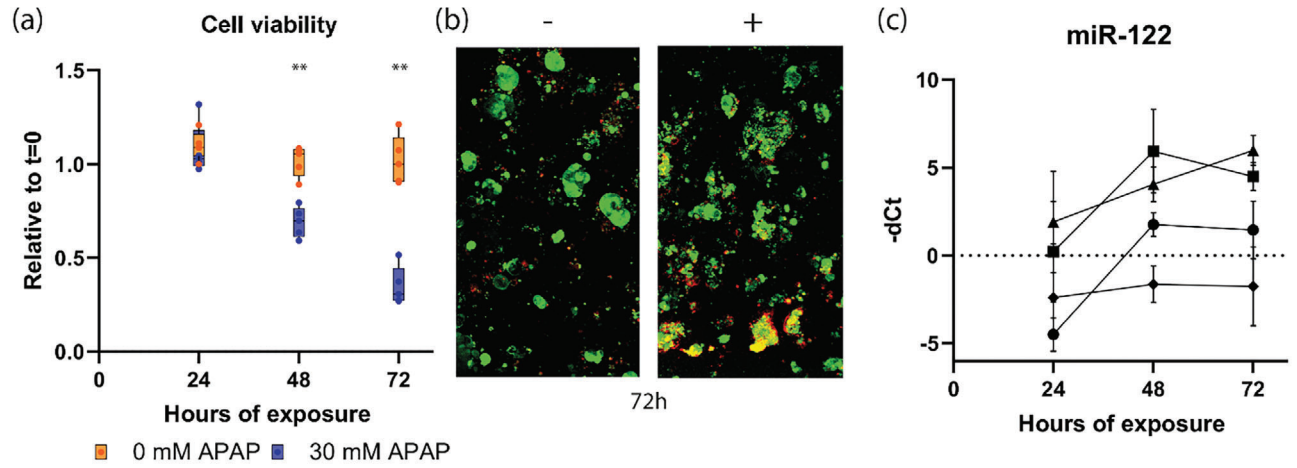

Figure 3. Acetaminophen (APAP) toxicity in bioprinted organoids. Exposure (72 h to 30 mMAPAP) started on day 7 post-printing with organoid-derived hepatocyte like cells. a) Cell viability of bioprinted organoids exposed to APAP relative to the cell viability at start of exposure. Bioprinted organoids exposed to 0 mM APAP (control; orange) and 30 mM (blue). Each dot represents the mean of a technical triplicate of one donor ($n = 5$). After 72 h of exposure, the cell viability of exposed organoids is significantly affected ($p < 0.01$). b) Live/dead staining of bioprinted organoids non-exposed (−, day 10 post-printing) and exposed to APAP for 72h (+, day 10 post-printing). Viable cells are stained in green, dead cells in red. c) Medium-levels of microRNA-122. Data are expressed as log2 fold-change (−ΔCt) using the non-exposed samples as baseline. Each symbol, representing a different donor ($n = 4$), and error bars represent the mean ± standard deviation.

features are still lacking resulting in an immature phenotype. By bioprinting, the biological resemblance of the in vitro system can be improved by applying precise patterning of organoids thereby permitting control over porosity and improved nutrient and waste exchange.[39–41] Here, we used extrusion-based bioprinting, which is an affordable technique in which a wide range of materials can be used.[42,43] The bioink (organoid-laden hydrogel pre-cursor) is pushed through a needle and is used to draw the desired 3D design layer-by-layer. Extrusion-based bioprinting could potentially cause organoid disruption due to shear stress at the nozzle. However, with the printing settings optimized in this study, viability of the hepatocyte-like cells from ICOs remained stable over time and comparable to non-printed controls.

Epithelial organoids are commonly cultured in the animal-derived and thermosensitive hydrogel Matrigel, which is advantageous for organoid growth and can be printed with a cooled print head.[44] However, while Matrigel has been well established to expand organoids in culture, using other 3D matrices during the organoid maturation steps has been proven to increase hepatic differentiation of liver organoids.[45,46] Furthermore, Matrigel shows considerable batch-to-batch variations, which represent a hurdle toward generation of highly standardized and scalable in vitro models for pharmaceutical research.[47] In our study, the main goal was to maintain a hepatic phenotype for subsequent testing, rather than proliferation and maintenance of undifferentiated phenotypes. Thus, we selected the widely used gelatin-derived hydrogel GelMA to prepare the printable bioinks. The modified methacryloyl groups in GelMA allow irreversible photocrosslinking and highly controllable stiffness of the hydrogel.[42] Furthermore, rheological analysis showed that the used GelMA concentration has shear thinning properties, which greatly facilitate stable extrusion while minimizing cell stress during printing.[48,49] Upon addition of organoids, the material still maintained its shear thinning properties. The selected GelMA concentration is known to give rise to relatively soft hydrogels, typically in the range ≈5 kPa.[50] Pluronic-127 was used to temporarily support the desired grid-like structure before photocrosslinking[51] and the sacrificial filaments can also serve as a template to provide channels suitable to permit vascularization at a later stage.[40] The porosity of the current lattice shaped constructs already permit close proximity of the liver organoids to the media and nutrient supply. LAP was used as photoinitiator for its cytocompatibility, herein demonstrated also when mixed with organoid-laden bioinks, and its potential to trigger crosslinking with visible light (≈405 nm), which has been shown to permit hydrogel formation under mild and cell-friendly photo-exposure conditions.[52] Importantly, this is, to the best of our knowledge, the first report demonstrating the feasibility of bioprinting organoids derived from liver epithelium. Such liver organoids, forming lumen-rich structures, are more structurally fragile than dense spheroids and could potentially be susceptible to damage and disruption during extrusion through a nozzle. This study indicates the feasibility and safety of bioprinting such structures without hampering their functionality and constitutes a necessary preliminary step for future studies of more complex bioprinted architectures. Taken together, extrusion-based bioprinting using GelMA in combination with a sacrificial material provide a versatile strategy for the bioprinting of a porous construct that sustains organoid viability.

Extrusion-based bioprinting of hepatic structures has been shown before using different hepatic in vitro models, such as tumor-derived hepatic lines,[39,40,53–55] (cryopreserved) PHHs,[56,57] and human iPSCs.[58,59] Although all cell-types have hepatocyte features, the cellular organization of these bioprinted models is different compared to the bioprinted organoid constructs. Cells can be bioprinted as single cells,[40,53–57,59] cellular aggregates that are forced to form (co-cultured) spheroids[39] or, in our case, as self-organizing organoids. Even though the size and level of organization of the cellular structures does not necessarily affect cell viability after bioprinting,[60] it can

have an effect on hepatic functionality[58] and contribute to cellular organization within prints. Extrusion-based bioprinted intestinal-derived organoids showed that specific patterning of the organoids can stimulate self-organization.[61] Here, liver organoids also reorganized within the bioprinted constructs and did not maintain their morphological characteristics as seen in Matrigel cultures. Even though there are morphological differences, the hepatic differentiation state in bioprinted constructs was similar compared to Matrigel. The high stability of the bioprinted organoids with respect to cell viability could also be due to intrinsic cell-binding motifs present in gelatin.[62]

Next to the stability in viability and gene expression levels, histology and function are equally important. The current liver constructs do not fully recapitulate the native liver structure yet. We showed that liver organoids can be patterned via bioprinting, which provides the basis for future applications. Several important steps need to be taken to increase the complexity of the in vitro system which will lead to improved hepatic differentiation. This improved differentiation can be reached by co-culture with supporting liver cells[63,64] or vascular cells leading to a vascularized construct,[40] or flow perfusion,[65,66] which can be applied to the bioprinted constructs.[11] The latter can be particularly beneficial, as recent studies have shown how in vitro zonation can be induced by flow perfusion.[67,68] The presence of Argininosuccinate synthetase (ASS, involved in urea cycle and mainly located in the periportal area) as well as the expression of CYP enzymes (mainly located in the perivenous area), suggests that hepatocyte-like cells from ICOs are not yet zonally oriented in the bioprinted constructs. In this study, we showed that hepatocyte-like cells from ICOs maintained high metabolic activity up to at least ten days after printing, allowing for post-printing exposure assays. The combination of bioprinting and ICOs provides possibilities to increase culture complexity to provide a more physiological relevant microenvironment and thereby potentially improve the hepatic differentiation state of the organoids.

Although several liver models have been developed for the determination of hepatic toxicity, almost all models have limitations that hamper their use in toxicity screening.[8] In this study, acetaminophen-induced toxicity was observed in the liver constructs over time, although used acetaminophen concentrations were relatively high compared to literature.[39,69] This is likely mainly due to the high level of the anti-oxidant glutathione present in the organoid differentiation medium which acts as an anti-oxidant and protects against APAP toxicity.[70] Additionally, expression levels of CYP2E1, which is mainly responsible for the formation of the toxic metabolite NAPQI (in addition CYP3A4 and CYP1A2 contribute to APAP metabolism, albeit to a lesser extent),[71] are only slightly increased in differentiated liver organoids compared to expanding conditions. Improved hepatic functionality, including CYP expression, can reinforce the predictive capacity for necrotic toxicity after formation of reactive metabolites.[72,73] With improvements of hepatic functionality of the organoids and the experimental set-up, bioprinted liver organoids could result in a robust in vitro model to detect drug-induced effects. Acetaminophen toxicity is known to be predictable and dose-dependent as the formation of a toxic metabolite causes toxicity, however most drug-induced hepatic injuries are less predictable and occur via different mechanisms.[74] By exposure of liver organoids to a selection of known hepatotoxic compounds with different toxicological mechanisms (for example formation of reactive metabolites, BSEP inhibition, mitochondrial impairment), the applicability of liver organoids in specific toxicological mechanisms can be established.[75]

4. Conclusion

We aimed to develop a hepatic model that allowed spatial control using hepatocyte-like cells from ICOs and gelatin-based hydrogel as bioink. By bioprinting epithelial organoids, we have taken the first step in the development of a more complex, and hence more physiologically relevant, in vitro model system that allows the accurate predictions of drug-induced liver injury (DILI). This study provided the basis of a humanized testing platform for personalized medicine and/or drug screening based on the creation of liver constructs through bioprinting.

5. Experimental Section

Cells and Culture Conditions: Healthy liver biopsies were obtained during liver transplantation at the Erasmus Medical Center Rotterdam in accordance with the ethical standard of the institutional committee to use the tissue for research purposes (ethical approval number MEC 2014–060). The procedure was in accordance with the Helsinki Declaration of 1975 and informed consent in writing was obtained from each patient. Obtained human liver material was frozen down in recovery cell freezing medium for future experiments or used for organoid isolation directly. Organoid isolation was performed as follows: Tissue was chopped into small pieces and enzymatically digested with 0.125 mg mL^{-1} Type II collagenase and 0.125 mg mL^{-1} dispase in Dulbecco's modified eagle's medium (DMEM) Glutamax supplemented with 0.01% (v/v) DNase I (Roche, Basel, Switzerland), 1% (v/v) fetal calf serum (FCS), and 1% (v/v) penicillin/streptomycin (P/S) at 37 °C. Every hour, the supernatant was collected and fresh enzyme-supplemented media was added to the remaining tissue until only ducts and single cells were visible. Cells were washed with DMEM Glutamax (supplemented with 1% (v/v) FCS and 1% (v/v) P/S) and spun down at 453 g for 5 min. All components were obtained from Life Technologies (Carlsbad, CA, USA).

The cell suspension was cultured in Matrigel (Corning, New York, NY, USA) droplets in expansion medium (EM) until intrahepatic cholangiocyte organoids (ICOs) arose, as previously described.[20] In short, EM consisted of Advanced DMEM/F12 (Life Technologies) supplemented with 1% (v/v) penicillin-streptomycin (Life Technologies), 1% (v/v) GlutaMax (Life Technologies), 10 mM HEPES (4-(2-hydroxyethyl)-1-piperazineethanesulfonic acid, Life Technologies), 2% (v/v) B27 supplement without vitamin A (Invitrogen, Carlsbad, CA, USA), 1% (v/v) N2 supplement (Invitrogen), 10 mM nicotinamide (Sigma–Aldrich, St Louis, MO, USA), 1.25 mM *N*-acetylcysteine (Sigma–Aldrich), 10% (v/v) R-spondin-1 conditioned medium (the Rspo1-Fc-expressing cell line was a kind gift from Calvin J. Kuo), 10 μM forskolin (Sigma–Aldrich), 5 μM A83-01 (transforming growth factor beta inhibitor; Tocris Bioscience, Bristol, UK), 50 ng mL^{-1} EGF (Invitrogen), 25 ng mL^{-1} HGF (Peprotech, Rocky Hill, NJ, USA), 0.1 μg mL^{-1} FGF10 (Peprotech), and 10 nM recombinant human (Leu15)-gastrin I (Sigma–Aldrich). Media were changed twice a week. Passaging occurred every 7–10 days at ratios ranging between 1:2 and 1:4. All cultures were kept in a humidified atmosphere of 95% air and 5% CO_2 at 37 °C. Organoids were primed for differentiation with BMP7 (25 ng mL^{-1}, Peprotech) through spiking EM 3 days prior to shifting to differentiation medium (DM). DM consisted of EM without R-spondin-1, FGF10 and nicotinamide, supplemented with 100 ng mL^{-1} FGF19 (Peprotech), 500 nM A83-01 (Tocris Bioscience), 10 μM DAPT (Selleckchem, Munich, Germany), 25 ng mL^{-1} BMP-7 (Peprotech), and 30 μM dexamethasone (Sigma–Aldrich). Organoids were kept on DM up to 10 days.

Bioink Preparation: Gelatin–methacryloyl (GelMA) was synthesized from gelatin-derived from porcine skin (Sigma–Aldrich) as previously described.[76] In short, 10% (w/v) gelatin in phosphate buffered saline (PBS) was reacted with 1:0.6 methacrylic anhydride (Sigma–Aldrich) at 50 °C for 1h in order to form 80% degree of functionalization of the lysine residues. The excess of methacrylic anhydride was removed by centrifugation. The obtained GelMA solution was neutralized with NaOH and dialyzed against distilled water for 5 days, sterile-filtered, freeze-dried, and stored at −20 °C until further use.

The used photoinitiator in the bioink was lithium-phenyl-2,4,6-trimethylbenzoylphosphinate (LAP; Sigma–Aldrich) 0.2% (w/v) dissolved in DMEM/F12 (without phenol red, supplemented with 1% (v/v) penicillin–streptomycin, 1% (v/v) GlutaMax, and 10 mM HEPES). Freeze-dried GelMA was dissolved (5% (w/v)) in the LAP-solution. The temperature of the GelMA solution was stabilized at 25 °C prior to cell mixing. Organoids were mechanically fragmented and mixed with the GelMA bioink right before transferring to the bioprinting cartridge. The sacrificial material Pluronic F-127 (Sigma–Aldrich) was dissolved in PBS (40% (w/v)) while incubating at 4 °C under continuous agitation.

Rheological Evaluation GelMA: The rheological properties of the hydrogel precursor solution were assessed using a DHR2 rheometer (TA Instruments, the Netherlands). To evaluate the hydrogels' shear thinning properties, a stainless-steel flat plate (diameter = 20 mm) with a 200 µm plate-to-plate distance was used. GelMA in LAP-solution (65 µL of 5% (w/v); previously described) was loaded and the gels' complex viscosity (Pa·S) was recorded at 25 °C as a function of shear rate (0.01–100 rad s^{-1}) at a constant strain of 5% (n = 3 for GelMA control, n = 4 for cell-laden GelMA).

Compound Diffusion in GelMA: A 5% (w/v) GelMA in 0.2% (w/v) LAP-solution was casted using a custom-designed PDMS mold and crosslinked for 10 min under 400 nm light exposure, to form cylindrical discs (diameter = 5 mm; height = 3 mm). To evaluate the diffusion rate of the crosslinked hydrogel construct, 10 µL of a green colored dye (MW = 5,343–561,7 g mol^{-1}; Singh Traders, Baambrugge, the Netherlands) was pipetted on top of the cylinder to create an even fluid layer over the top face surface of the hydrogel disc. After 1, 2, 4, 6, 8, 12, 16, 24, 32 min, samples were removed from the mold (n = 2 per time point). The migration of the dye through the gel over time was assessed using a stereomicroscope (Olympus SZ61 coupled with an Olympus DP70 digital camera; Olympus Soft Imaging Solutions GmbH, the Netherlands) by imaging cross-sections of the hydrogel cylinder at the indicated time points.

Bioprinting Settings: The constructs were designed using a computer aided design (CAD) software (BioCAD, RegenHU, Switzerland), and printed using an extrusion-based bioprinter (3D Discovery, RegenHU, Switzerland) in a sterile 5 cm petri dish (ThermoFisher, Waltham, Massachusetts, USA). The constructs consist of horizontal strands of Pluronic F-127 with 0.135 mm space between each strand. In between these supporting strands, the cell-laden GelMA was printed and photocrosslinked with an exposure of 45 s with blue-light (405 nm). Subsequent layers were printed in a layer-by-layer fashion, with a 90 ° rotation in the filament orientation between each layer. Pluronic F-127 was printed at a speed of 30 mm s^{-1} at a pressure of 450–550 kPa. GelMA was printed at a speed of 15 mm s^{-1} at a pressure of 15–30 kPa. The printhead containing the cell-laden GelMA bioink was equipped with a cooling device set to 25 °C. The dispensing tip was a stainless steel 27G nozzle (length 6.35 mm; Nordson, Westlake, OH, USA) for both bioinks. After printing ten layers, the printed construct was further photocrosslinked for 10 min in a custom-made curing box containing 400 nm LED lights (000214, Groenlicht, Geldrop, the Netherlands). Pluronic F-127 was washed away with DMEM/F12 (without phenol red, supplemented with 1% (v/v) penicillin-streptomycin, 1% (v/v) GlutaMax, 10 mM HEPES) at 4 °C resulting in porous cubical shaped constructs (≈5 × 5 × 2 mm, l × w × h). Constructs were cultured in 24 well plates (ThermoFisher) under differentiating conditions (Differentiation Medium, DM) as described for a maximum of 10 days in a humidified atmosphere of 95% air and 5% CO_2 at 37 °C.

Alamar Blue Cell Viability Assay: Cell viability of the organoids (four donors in technical triplicate) in printed constructs and plated controls (GelMA and Matrigel) was examined through an Alamar Blue assay (ThermoFisher), a resazurin-based solution that functions as a cell health indicator. Briefly, the Alamar Blue reagent was diluted 1:10 in DMEM/F12 (phenol-red free). Cells were incubated for 2 h at 37 °C. Subsequently, fluorescence intensity of the Alamar Blue solution was measured with a photospectrometer (Fluoroskan Ascent FL, ThermoFischer Scientific) at ex/em 544/570 nm.

Cell Viability: Cell viability of printed and exposed organoids was visualized using a LIVE/DEAD Viability/Cytotoxicity Kit for mammalian cells (ThermoFisher, Catalog number: L3224). Samples were incubated with fluorescent dyes to detect live (Calcein-AM) and dead (Ethidium homodimer-1) cells. Samples were imaged using confocal laser scanning microscopy (SP8, Leica Microsystems, the Netherlands).

Gene Expression: Prior to RNA isolation, GelMA hydrogels were broken down using QIAshredder columns according to the manufacturer's instructions (Qiagen, Hilden, Germany). RNA was isolated from liver organoids (four donors (n = 4), in triplicate) using 350 µL RNeasy lysis buffer directly added into one well of the 24 well plate followed by RNA extraction using the RNeasy micro Kit according to the manufacturer's instructions (Qiagen). cDNA synthesis was performed using iScript cDNA synthesis kit (Bio-Rad, Veenendaal, the Netherlands). Relative gene expression of selected genes was measured using RT-qPCR in a CFX-384 (Bio-Rad). Primer design, validation, RT-qPCR conditions, and data analysis was performed as previously described.[77] Normalization was performed using reference genes *GAPDH* and *RPS5*. Details of primers are listed in Table S1, Supporting Information.

Immunofluorescence: Organoids (four donors) were fixed in 4% (w/v) paraformaldehyde (PFA) with 0.1% (v/v) eosin and stored in 70% (v/v) EtOH at 4 °C until further processing. Bioprinted constructs were placed in agarose before embedding to keep the constructs integrity during the histological processing. Samples were embedded in paraffin and cut into 4 µm sections. Sections were deparaffinized and rehydrated. After antigen retrieval (information per antibody in Table S2, Supporting Information), a blocking step was performed using 10% (v/v) normal goat serum (Bio-Rad) in PBS for 30 min at RT. Antibodies are listed in Table S2, Supporting Information. Incubation with primary antibodies was performed overnight at 4 °C. Secondary antibodies were incubated at room temperature for 1 h. Nuclei were stained with DAPI (Sigma–Aldrich) diluted 2,000× in PBS. Washing steps were performed using a buffer of PBS with 0.1% Triton X-100 (Sigma–Aldrich) and 0.2% (w/v) Bovine Serum Albumin (Sigma). Slides were mounted using FluorSave (Merck-Millipore, Burlington, MA, USA), and images were acquired using confocal microscopy (SP8, Leica Microsystems).

HE Staining: Morphology and distribution of organoids in printed constructs (four donors) was evaluated by hematoxylin and eosin (H&E) staining, scanned with slide scanner (Hamamatsu Photonics, Hamamatsu-city, Japan).

Acetaminophen Toxicity: Acetaminophen (APAP; CAS 103-90-2, Sigma–Aldrich) was dissolved in differentiation medium as described above, using DMEM Glutamax with added factors as described for DM except Glutamax, NAC, and B27. At day 7 of differentiation, organoids were exposed to 30 mM APAP for 72 h (four donors, n = 3), repeating dosing every 24h. Metabolic activity was examined at 24, 48, and 72 h after start of exposure using the Alamar Blue assay. Medium was collected at 4, 24, 48, and 72h of exposure to examine levels of miRNA-122 in the medium.

Detection miRNA-122 in Medium: Total RNA was extracted from assay medium (120–160 µL) using the miRNeasy Serum/Plasma Kit (Qiagen) following the manufacturer's instructions. miRNA-122 was reverse-transcribed using the miScript II RT Kit (Qiagen) according to the manufacturer's protocol. Normalization of qPCR data of printed samples was performed using spiked-in synthetic C. elegans miR-39 (miRNeasy Serum/Plasma Spike-In Control, Qiagen). Ce_miR-39_1 and H2_miR-122a_1 miScript Primer Assays (Qiagen) were used for qPCR. The qPCR was carried out in a CFX-384 (Bio-Rad). Calculations were performed as previously described.[78] Changes of miRNA levels in supernatants were determined by comparing the Ct values in the exposed samples to the control (non-exposed) samples and expressed as −ΔCt.

Statistical Analysis: For the statistical analysis of metabolic activity data, the gene expression data and the effects of acetaminophen exposure, the authors applied the post-hoc comparison uncorrected Dunn's test using GraphPad Prism (version 8.3.0). Significance levels are * $p \leq 0.05$; ** $p \leq 0.01$ and *** $p \leq 0.001$.

Supporting Information

Supporting Information is available from the Wiley Online Library or from the author.

Acknowledgements

This work is part of the research program Applied and Engineering Sciences with project number 15498, which is financed by the Dutch Research Council (NWO). R.L. acknowledges funding from the European Research Council (ERC) under the European Union's Horizon 2020 research and innovation programme (grant agreement No. 949806 and No. 964497) and the Gravitation Program "Materials Driven Regeneration", funded by the Dutch Research Council (NWO), project number 024.003.013.

Conflict of Interest

The authors declare no conflict of interest.

Data Availability Statement

Research data are not shared.

Keywords

drug induced liver injury, extrusion-based bioprinting, in vitro modeling, organoids

Received: September 2, 2021
Published online: October 5, 2021

[1] V. B. Siramshetty, J. Nickel, C. Omieczynski, B.-O. Gohlke, M. N. Drwal, R. Preissner, *Nucleic Acids Res.* **2016**, *44*, D1080.
[2] W. M. Lee, *N. Engl. J. Med.* **2003**, *349*, 474.
[3] G. Ostapowicz, R. J. Fontana, F. V. Schiødt, A. Larson, T. J. Davern, S. H. Han, T. M. McCashland, A. O. Shakil, J. E. Hay, L. Hynan, J. S. Crippin, A. T. Blei, G. Samuel, J. Reisch, W. M. Lee, U.S. Acute Liver Failure Study Group, *Ann. Intern. Med.* **2002**, *137*, 947.
[4] M. R. Mcgill, H. Jaeschke, *Biochim. Biophys. Acta, Mol. Basis Dis.* **2019**, *1865*, 1031.
[5] F. Ballet, *Dig.. Dis.* **2015**, *33*, 477.
[6] H. Olson, G. Betton, D. Robinson, K. Thomas, A. Monro, G. Kolaja, P. Lilly, J. Sanders, G. Sipes, W. Bracken, M. Dorato, K. Van Deun, P. Smith, B. Berger, A. Heller, *Regul. Toxicol. Pharmacol.* **2000**, *32*, 56.
[7] M. J. Gómez-Lechón, L. Tolosa, I. Conde, M. T. Donato, *Expert Opin. Drug Metab. Toxicol.* **2014**, *10*, 1553.
[8] P. Godoy, N. J. Hewitt, U. Albrecht, M. E. Andersen, N. Ansari, S. Bhattacharya, J. G. Bode, J. Bolleyn, C. Borner, J. Böttger, A. Braeuning, R. A. Budinsky, B. Burkhardt, N. R. Cameron, G. Camussi, C.-S. Cho, Y.- J. Choi, J. Craig Rowlands, U. Dahmen, G. Damm, O. Dirsch, M. T. Donato, J. Dong, S. Dooley, D. Drasdo, R. Eakins, K. S. Ferreira, V. Fonsato, J. Fraczek, R Gebhardt, et al., *Arch. Toxicol.* **2013**, *87*, 1315.
[9] V. M. Lauschke, R. Z. Shafagh, D. F. G. Hendriks, M. Ingelman-Sundberg, *Biotechnol. J.* **2019**, *14*, 1800347.
[10] J. Fraczek, J. Bolleyn, T. Vanhaecke, V. Rogiers, M. Vinken, *Arch. Toxicol.* **2013**, *87*, 577.
[11] M. Ruoß, M. Vosough, A. Königsrainer, S. Nadalin, S. Wagner, S. Sajadian, D. Huber, Z. Heydari, S. Ehnert, J. G. Hengstler, A. K. Nussler, *Food Chem. Toxicol.* **2020**, *138*, 111188.
[12] J. V. Castell, R. Jover, C. P. Martnez-Jimnez, M. J. Gmez-Lechn, *Expert Opin. Drug Metab. Toxicol.* **2006**, *2*, 183.
[13] S. N. Hart, Y. Li, K. Nakamoto, E.-A. Subileau, D. Steen, X-Bo Zhong, *Drug Metab. Dispos.* **2010**, *38*, 988.
[14] M. N. Ashraf, M. W. Asghar, Y. Rong, M. R. Doschak, T. K. L. Kiang, *Eur. J. Drug Metab. Pharmacokinet.* **2018**, *44*, 437.
[15] S.-F. Zhou, J.-P. Liu, B. Chowbay, *Drug Metab. Rev.* **2009**, *41*, 89.
[16] F. Schutgens, H. Clevers, *Annu. Rev. Pathol.: Mech. Dis.* **2020**, *15*, 211.
[17] A. Marsee, F. J. M. Roos, M. M. A. Verstegen, H. Gehart, E. De Koning, F. Lemaigre, S. J. Forbes, W. C. Peng, M. Huch, T. Takebe, L J. W. Van Der Laan, B. Spee, A. Marsee, HPB Organoid Consortium, *Cell Stem Cell* **2021**, *28*, 816.
[18] T. Sato, R. G. Vries, H. J. Snippert, M. Van De Wetering, N. Barker, D. E. Stange, J. H. Van Es, A. Abo, P. Kujala, P. J. Peters, H. Clevers, *Nature* **2009**, *459*, 262.
[19] L. Planas-Paz, T. Sun, M. Pikiolek, N. R. Cochran, S. Bergling, V. Orsini, Z. Yang, F. Sigoillot, J. Jetzer, M. Syed, M. Neri, S. Schuierer, L. Morelli, P. S. Hoppe, W. Schwarzer, C. M. Cobos, J. L. Alford, L. Zhang, R. Cuttat, A. Waldt, N. Carballido-Perrig, et al., *Cell Stem Cell* **2019**, *25*, 39.
[20] M. Huch, H. Gehart, R. Van Boxtel, K. Hamer, F. Blokzijl, M, M. A. Verstegen, E. Ellis, M. Van Wenum, S A. Fuchs, J. De Ligt, M. Van De Wetering, N. Sasaki, S J. Boers, H. Kemperman, J. De Jonge, J N. M. Ijzermans, E E. S. Nieuwenhuis, R. Hoekstra, S. Strom, R R. G. Vries, L J. W. Van Der Laan, et al., *Cell* **2015**, *160*, 299.
[21] K. Schneeberger, N. Sánchez-Romero, S. Ye, F. G. van Steenbeek, L. A. Oosterhoff, I. Pla Palacin, C. Chen, M. E. van Wolferen, G. van Tienderen, R. Lieshout, H. Colemonts-Vroninks, I. Schene, R. Hoekstra, M. M. A. Verstegen, L. J. W. van der Laan, L. C. Penning, S. A. Fuchs, H. Clevers, J. de Kock, P. M. Baptista, B. Spee, *Hepatology* **2020**, *72*, 257.
[22] C. Chen, A. Soto-Gutierrez, P. M. Baptista, B. Spee, *Gastroenterology* **2018**, *154*, 1258.
[23] G. H. Underhill, S. R. Khetani, *CMGH* **2018**, *5*, 426.
[24] K. Schneeberger, B. Spee, P. Costa, N. Sachs, H. Clevers, J. Malda, *Biofabrication* **2017**, *9*, 013001.
[25] K. T. Lawlor, J. M. Vanslambrouck, J. W. Higgins, A. Chambon, K. Bishard, D. Arndt, P. X. Er, S. B. Wilson, S E. Howden, K. S. Tan, F. Li, L J. Hale, B. Shepherd, S. Pentoney, S. C. Presnell, A. E. Chen, M. H. Little, *Nat. Mater.* **2020**, *20*, 260.
[26] R. Levato, T. Jungst, R. G. Scheuring, T. Blunk, J. Groll, J. Malda, *Adv. Mater.* **2020**, *32*, 1906423.
[27] C. Chen, A. Soto-Gutierrez, P M. Baptista, B. Spee, *Gastroenterology* **2018**, *154*, 1258.
[28] T. Takahashi, *Annu. Rev. Pharmacol. Toxicol.* **2019**, *59*, 447.
[29] H. Jaeschke, M. L. Bajt, A. Ramachandran, *Mechanisms of Acetaminophen Hepatotoxicity: Cell Death Signaling Mechanisms in Hepatocytes*, Elsevier, New York, NY **2017**.
[30] S. C. Ramaiahgari, M. W. Den Braver, B. Herpers, V. Terpstra, J. N. M. Commandeur, B. Van De Water, L. S. Price, *Arch. Toxicol.* **2014**, *88*, 1083.
[31] D. Utkarsh, C. Loretz, A. P. Li, *Chem.-Biol. Interact.* **2016**, *255*, 12.
[32] T. Takahashi, *Annu. Rev. Pharmacol. Toxicol.* **2019**, *59*, 447.
[33] H. S. Kruitwagen, L. A. Oosterhoff, I. G. W. H. Vernooij, I. M. Schrall, M. E. Van Wolferen, F. Bannink, C. Roesch, L. Van Uden, M. R. Molenaar, J. B Helms, G, C. M. Grinwis, M. M. A. Verstegen, L. J. W. Van Der Laan, M. Huch, N. Geijsen, R. G. Vries, H. Clevers, J. Rothuizen, B. A. Schotanus, L. C. Penning, B. Spee, *Stem Cell Rep.* **2017**, *8*, 822.

[34] I. F. Schene, I. P. Joore, R. Oka, M. Mokry, A. H. M. Van Vugt, R. Van Boxtel, H. P. J. Van Der Doef, L. J. W. Van Der Laan, M. M. A. Verstegen, P. M. Van Hasselt, E. E. S. Nieuwenhuis, S. A. Fuchs, *Nat. Commun.* **2020**, *11*, 5352.
[35] F. Sampaziotis, D. Muraro, O. C. Tysoe, S. Sawiak, T. E. Beach, E. M. Godfrey, S. S. Upponi, T. Brevini, B T. Wesley, J. Garcia-Bernardo, K. Mahbubani, G. Canu, R. Gieseck, N L. Berntsen, V L. Mulcahy, K. Crick, C. Fear, S. Robinson, L. Swift, L. Gambardella, et al., *Science* **2021**, *371*, 839.
[36] F. J. M. Roos, M. M. A. Verstegen, L. Muñoz Albarinos, H. P. Roest, J.-W. Poley, G. W. M. Tetteroo, J. N. M. Ijzermans, L. J. W. Van Der Laan, *Front. Cell Dev. Biol.* **2021**, *8*, 630492.
[37] F. Schutgens, M. B. Rookmaaker, T. Margaritis, A. Rios, C. Ammerlaan, J. Jansen, L. Gijzen, M. Vormann, A. Vonk, M. Viveen, F. Y. Yengej, S. Derakhshan, K M. De Winter-De Groot, B. Artegiani, R. Van Boxtel, E. Cuppen, A P. A. Hendrickx, M M. Van Den Heuvel-Eibrink, E. Heitzer, H. Lanz, J. Beekman, et al., *Nat. Biotechnol.* **2019**, *37*, 303.
[38] T. Sato, D. E. Stange, M. Ferrante, R. G. J. Vries, J. H. Van Es, S. Van Den Brink, W. J. Van Houdt, A. Pronk, J. Van Gorp, P. D. Siersema, H. Clevers, *Gastroenterology* **2011**, *141*, 1762.
[39] N. S. Bhise, V. Manoharan, S. Massa, A. Tamayol, M. Ghaderi, M. Miscuglio, Qi Lang, Y. Shrike Zhang, S. R. Shin, G. Calzone, N. Annabi, T. D. Shupe, C. E. Bishop, A. Atala, M. R. Dokmeci, A. Khademhosseini, *Biofabrication* **2016**, *8*, 014101.
[40] S. Massa, M. A. Sakr, J. Seo, P. Bandaru, A. Arneri, S. Bersini, E. Zare-Eelanjegh, E. Jalilian, B.-H. Cha, S. Antona, A. Enrico, Y. Gao, S. Hassan, J. P. Acevedo, M R. Dokmeci, Y. S. Zhang, A. Khademhosseini, S. R. Shin, *Biomicrofluidics* **2017**, *11*, 044109.
[41] T. Grix, A. Ruppelt, A. Thomas, A.-K. Amler, B. Noichl, R. Lauster, L. Kloke, *Genes* **2018**, *9*, 176.
[42] B. J. Klotz, D. Gawlitta, A. J. W. P. Rosenberg, J. Malda, F. P. W. Melchels, *Trends Biotechnol.* **2016**, *34*, 394.
[43] I. T. Ozbolat, M. Hospodiuk, *Biomaterials* **2016**, *76*, 321.
[44] J. E. Snyder, Q. Hamid, C. Wang, R. Chang, K. Emami, H. Wu, W. Sun, *Biofabrication* **2011**, *3*, 034112.
[45] M. Krüger, L. A. Oosterhoff, M. E. van Wolferen, S. A. Schiele, A. Walther, N. Geijsen, L. De Laporte, L. J. W. van der Laan, L. M. Kock, B. Spee, *Adv. Healthcare Mater.* **2020**, *9*, e1901658.
[46] B. J. Klotz, L. A. Oosterhoff, L. Utomo, K. S. Lim, Q. Vallmajo-Martin, H. Clevers, T. B. F. Woodfield, A. J. W. P. Rosenberg, J. Malda, M. Ehrbar, B. Spee, D. Gawlitta, *Adv. Healthcare Mater.* **2019**, *8*, 1900979.
[47] G. Benton, I. Arnaoutova, J. George, H. K. Kleinman, J. Koblinski, *Adv. Drug Delivery Rev.* **2014**, *79–80*, 3.
[48] T. Jungst, W. Smolan, K. Schacht, T. Scheibel, J. Groll, *Chem. Rev.* **2016**, *116*, 1496.
[49] A. Schwab, R. Levato, M. D'este, S. Piluso, D. Eglin, J. Malda, *Chem. Rev.* **2020**, *120*, 11028.
[50] W. Schuurman, P. A. Levett, M. W. Pot, P. R. Van Weeren, W. J. A. Dhert, D. W. Hutmacher, F. P. W. Melchels, T J. Klein, J. Malda, *Macromol. Biosci.* **2013**, *13*, 551.
[51] R. Levato, W. R. Webb, I. A. Otto, A. Mensinga, Y. Zhang, M. Van Rijen, R. Van Weeren, I M. Khan, J. Malda, *Acta Biomater.* **2017**, *61*, 41.
[52] A K. Nguyen, P L. Goering, V. Reipa, R J. Narayan, *Biointerphases* **2019**, *14*, 021007.
[53] L. E. Bertassoni, J. C. Cardoso, V. Manoharan, A. L. Cristino, N. S. Bhise, W. A. Araujo, P. Zorlutuna, N. E. Vrana, A. M. Ghaemmaghami, M. R. Dokmeci, A. Khademhosseini, *Biofabrication* **2014**, *6*, 024105.
[54] T. Hiller, J. Berg, L. Elomaa, V. Röhrs, I. Ullah, K. Schaar, A. C. Dietrich, M. A. Al-Zeer, A. Kurtz, A. C. Hocke, S. Hippenstiel, H. Fechner, M. Weinhart, J. Kurreck, *Int. J. Mol. Sci.* **2018**, *19*, 3129.
[55] M. Gori, S. M. Giannitelli, M. Torre, P. Mozetic, F. Abbruzzese, M. Trombetta, E. Traversa, L. Moroni, A. Rainer, *Adv. Healthcare Mater.* **2020**, *6*, 2001163.
[56] A. Mazzocchi, M. Devarasetty, R. Huntwork, S. Soker, A. Skardal, *Biofabrication* **2018**, *11*, 015003.
[57] L. M. Norona, D. G. Nguyen, D. A. Gerber, S. C. Presnell, E. L. Lecluyse, *Toxicol. Sci.* **2016**, *154*, 354.
[58] E. Goulart, L. C. De Caires-Junior, K. A. Telles-Silva, B. H. S. Araujo, S. A. Rocco, M. Sforca, I. L. De Sousa, G. S. Kobayashi, C. M. Musso, A. F. Assoni, D. Oliveira, E. Caldini, S. Raia, P. I. Lelkes, M. Zatz, *Biofabrication* **2020**, *12*, 015010.
[59] A. Faulkner-Jones, C. Fyfe, D.-J. Cornelissen, J. Gardner, J. King, A. Courtney, W. Shu, *Biofabrication* **2015**, *7*, 044102.
[60] C. D. Roche, P. Sharma, A. W. Ashton, M. Xue, C. Gentile, C. Jackson, *Front. Bioeng. Biotechnol.* **2021**, *9*, 110.
[61] J. A. Brassard, M. Nikolaev, T. Hübscher, M. Hofer, M P. Lutolf, *Nat. Mater.* **2020**, *20*, 22.
[62] N. Davidenko, C. F. Schuster, D. V. Bax, R. W. Farndale, S. Hamaia, S. M. Best, R. E. Cameron, *J. Mater. Sci.: Mater. Med.* **2016**, *27*, 148.
[63] H. Lee, S. Chae, J. Y. Kim, W. Han, J. Kim, Y. Choi, D.-W. Cho, *Biofabrication* **2018**, *11*, 025001.
[64] X. Ma, C. Yu, P. Wang, W. Xu, X. Wan, C. S. E. Lai, J. Liu, A. Koroleva-Maharajh, S. Chen, *Biomaterials* **2018**, *185*, 310.
[65] S. S. Bale, J. T. Borenstein, *Drug Metab. Dispos.* **2018**, *46*, 1638.
[66] A. J. Foster, B. Chouhan, S. L. Regan, H. Rollison, S. Amberntsson, L. C. Andersson, A. Srivastava, M. Darnell, J. Cairns, S. E. Lazic, K.-J. Jang, D. B. Petropolis, K. Kodella, J. E. Rubins, D. Williams, G. A. Hamilton, L. Ewart, P. Morgan, *Arch. Toxicol.* **2019**, *93*, 1021.
[67] J. W. Allen, *Toxicol. Sci.* **2005**, *84*, 110.
[68] J. Ahn, J. Ahn, S. Yoon, Y. S. Nam, M. Y. Son, J. H. Oh, *J Biol Eng.* **2019**, *13*, 22.
[69] Y. Zhou, J. X. Shen, V. M. Lauschke, *Front. Pharmacol.* **2019**, *10*, 1093.
[70] J. Xu, S. Oda, T. Yokoi, *Toxicol. In Vitro* **2018**, *48*, 286.
[71] E. Yoon, A. Babar, M. Choudhary, M. Kutner, N. Pyrsopoulos, *J. Clin. Transl. Hepatol.* **2016**, *4*, 131.
[72] C. Lin, S. R. Khetani, *Biomed Res. Int.* **2016**, *2016*, 1829148.
[73] A. J. S. Ribeiro, X. Yang, V. Patel, R. Madabushi, D. G. Strauss, *Clin. Pharmacol. Ther.* **2019**, *106*, 139.
[74] C. Goldring, A. Norris, N. Kitteringham, M. D. Aleo, D J. Antoine, J. Heslop, B. A. Howell, M. Ingelman-Sundberg, R. Kia, L. Kamalian, S. Koerber, J.-C. Martinou, A. Mercer, J. Moggs, D. J. Naisbitt, C. Powell, J. Sidaway, R. Sison-Young, J. Snoeys, B. Van De Water, et al., *Appl. In Vitro Toxicol.* **2015**, *1*, 175.
[75] S. Dragovic, N. P. E. Vermeulen, H. H. Gerets, P. G. Hewitt, M. Ingelman-Sundberg, B. K. Park, S. Juhila, J. Snoeys, R. J. Weaver, *Arch. Toxicol.* **2016**, *90*, 2979.
[76] F. P. W. Melchels, M. M. Blokzijl, R. Levato, Q. C. Peiffer, M. D. Ruijter, W. E. Hennink, T. Vermonden, J. Malda, *Biofabrication* **2016**, *8*, 035004.
[77] F. G. Van Steenbeek, B. Spee, L. C. Penning, A. Kummeling, I. H. M. Van Gils, G. C. M. Grinwis, D. Van Leenen, F. C. P. Holstege, M. Vos-Loohuis, J. Rothuizen, P. A. J. Leegwater, *PLoS One* **2013**, *8*, e57973.
[78] E. M. Kroh, R. K. Parkin, P. S. Mitchell, M. Tewari, *Methods* **2010**, *50*, 298.